Microchannel Thermal Management System With Two-Phase Flow for Power Electronics Over 500 W/cm^2 Heat Dissipation

Fengze Hou, Hengyun Zhang, Dezhu Huang, Jiajie Fan, *Senior Member, IEEE*, Fengman Liu, Tingyu Lin, Liqiang Cao, Xuejun Fan, *Fellow, IEEE*, Braham Ferreira, *Fellow, IEEE*, and Guoqi Zhang, *Fellow, IEEE*

***Abstract*—In this article, a microchannel thermal management system (MTMS) with the two-phase flow using the refrigerant R1234yf with low global warming potential is presented. The thermal test vehicles (TTVs) were made of either single or multiple thermal test chips embedded in the substrates, which were then attached to the MTMS. The system included two identical aluminum microchannel heat sinks (MHSs) connected in series in the cooling loop, which also consisted of a gas flowmeter, a miniature compressor, a condenser, a throttling device, and accessory measurement components. The experimental results showed that the thermal management system could dissipate a heat flux of 526 W/cm^2 while maintaining the junction temperature below 120 °C. For SiC MOSFET with a higher junction temperature, e.g., 175 °C, the current system is expected to dissipate a heat flux as high as about 750 W/cm^2. The effects of the rotational speed of the compressor, the opening of the throttling device, TTV layout on MHS, and a downstream heater on the cooling performance of the system were analyzed in detail. The study shows that the present thermal management with a two-phase flow system is a promising cooling technology for the high heat flux SiC devices.**

***Index Terms*—Microchannel thermal management system (MTMS), two-phase flow, R1234yf, power electronics, SiC MOSFET.**

Manuscript received December 12, 2019; revised March 2, 2020; accepted March 27, 2020. Date of publication April 5, 2020; date of current version June 23, 2020. This work was supported in part by the National Natural Science Foundation of China under Grants U1730143 and 51876113 and in part by the Key-Area Research and Development Program of GuangDong Province under Project 2019B010131001. Recommended for publication by Associate Editor M. Chen. *(Corresponding authors: Hengyun Zhang; Xuejun Fan; and Guoqi Zhang.)*

Fengze Hou is with the Institute of Microelectronics of Chinese Academy of Sciences, Beijing 100029, China, with the Department of Microelectronics, Delft University of Technology, Delft CT 2628, The Netherlands, and also with the National Center for Advanced Packaging, Wuxi 214135, China (e-mail: f.hou-1@tudelft.nl; houfengze@ime.ac.cn).

Hengyun Zhang and Dezhu Huang are with the School of Mechanical and Automotive Engineering, Shanghai University of Engineering Science, Shanghai 201620, China (e-mail: zhanghengyun@sues.edu.cn; m060118149@sues.edu.cn).

Jiajie Fan and Guoqi Zhang are with the Department of Microelectronics, Delft University of Technology, Delft, CT 2628, The Netherlands (e-mail: j.fan-1@tudelft.nl; g.q.zhang@tudelft.nl).

Fengman Liu and Liqiang Cao are with the Institute of Microelectronics of Chinese Academy of Sciences, Beijing 100029, China, and with the National Center for Advanced Packaging, Wuxi 214135, China (e-mail: liufengman@ime.ac.cn; caoliqiang@ime.ac.cn).

Tingyu Lin is with the National Center for Advanced Packaging, Wuxi 214135, China (e-mail: tingyulin@ncap-cn.com).

Xuejun Fan is with the Department of Mechanical Engineering, Lamar University, Beaumont, TX 77710 USA (e-mail: xuejun.fan@lamar.edu).

Braham Ferreira is with the Department of Telecommunication Engineering, University of Twente, Enschede NB 7522, The Netherlands (e-mail: j.a.ferreira@utwente.nl).

Color versions of one or more of the figures in this article are available online at http://ieeexplore.ieee.org.

Digital Object Identifier 10.1109/TPEL.2020.2985117

I. Introduction

THE heat flux of the next-generation silicon insulated-gate bipolar transistor (Si IGBT) used in pure and hybrid electric vehicle applications would be as high as 500 W/cm^2, more than three times of heat flux in comparison with the current level of 100–150 W/cm^2 [1]–[3]. As a promising wide-bandgap device, silicon carbide metal–oxide–semiconductor field-effect transistor (SiC MOSFET) has many advantages such as higher breakdown voltage, higher switching frequency, and lower switching loss [4]. As its form factor tends to be smaller, its heat flux can reach up to 1 kW/cm^2 in comparison with Si IGBT with the same voltage blocking capability [4]–[6].

Such high heat fluxes cannot be addressed by using conventional cooling solutions, such as vapor chamber [7], [8], and single-phase liquid cooling [9]–[12]. Vapor chamber in combination with forced convection could dissipate heat flux no more than 100 W/cm^2 [13], while single-phase liquid cooling could reach 350 W/cm^2 [14]–[16]. Recently, immersion pool boiling and liquid metal cooling schemes have been reported for high heat flux electronics [13], [18]–[20]. The immersion pool boiling, which requires dielectric fluid to be in contact with the ICs directly, is usually limited by the critical heat flux of dielectric fluid and, thus, has insufficient cooling capacity. The liquid metal has much better thermophysical properties using eutectic alloys of different materials such as gallium, indium, and tin [20], but it may not be compatible with the metal piping and fittings. The cost of liquid metal is also much higher in comparison with other coolants [21].

Two-phase flow boiling regimes have received extensive attention in power electronics applications in recent years. Taking advantage of the latent heat of liquid refrigerant during its boiling process, it can provide higher heat transfer coefficients, lower flow rates, more uniform surface temperatures, and lower pumping power than a single-phase cooling scheme [1], [22]–[24]. However, the refrigerant boiling requires a wise control of the pressure and temperature of the refrigerant in the evaporator so

that the isothermal heat absorption can be achieved during the flow boiling process.

Much research effort has been devoted to the two-phase flow boiling in the microchannel thermal management system (MTMS) for electronics cooling [25]–[28]. R134a is commonly used refrigerant. In our previous study [28], an experimental study of a compact two-phase cooling system using R134a as a refrigerant was performed for high heat flux electronic packages. The experimental results showed the evaporator system could dissipate over 380 W/cm^2 for the thermal test vehicle (TTV) while maintaining its temperature at about 90 °C.

Although R134a is a chlorine-free and non-ozone-depleting hydrofluorocarbon refrigerant, it has relatively high global warming potential (GWP) of 1430, which are several orders of magnitude greater than CO_2, and has been banned in Europe for new mobile air conditioner [29]. According to the latest EU F-gas Regulation, all F-gases with GWP of more than 150 will be banned as the refrigerant or foam blowing agent in any hermetically sealed system from 2022 [30].

On the other hand, R1234yf has a GWP of only 4, which is much lower than R134a and has been adopted in Europe and is being proposed to replace R134a in some countries [30]–[32]. There are some reports on experimental studies of R1234yf as a drop-in replacement for R134a in an MTMS [29]–[32]. Nonetheless, there is little work reported on two-phase flow boiling heat transfer of R1234yf in a microchannel heat sink (MHS) for high heat-flux power electronics cooling.

In this article, an MTMS with the two-phase flow for power electronics is presented. Si-based TTVs were designed and fabricated to evaluate the cooling performance of the proposed thermal management system. Environment-friendly refrigerant R1234yf with low boiling points was selected to fill the system. The system mainly consisted of two identical aluminum (Al) MHSs, a miniature compressor, a condenser, a throttling device, and accessory measurement components. The cooling performance of the system with one single-chip TTV was first analyzed. Then, the effects of the rotational speed of the compressor, the opening of the throttling device, TTV layout on MHS, and a downstream heater on the cooling performance of the system were analyzed sequentially. Finally, the performance potential of the thermal management system was also discussed.

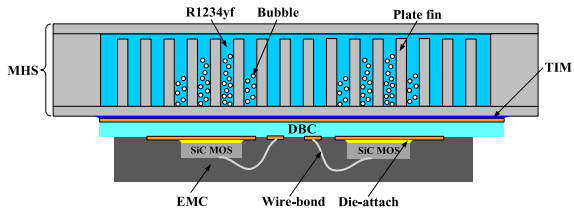

Fig. 1. Schematic of the SiC power module assembled on the MHS with two-phase flow boiling.

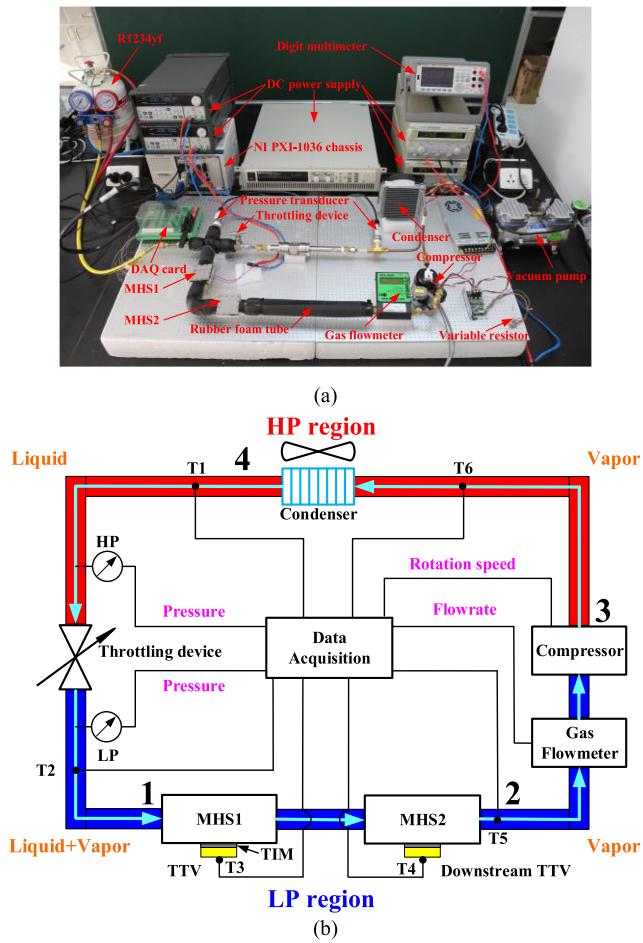

Fig. 2. MTMS. (a) Experimental measurement platform. (b) Schematic diagram.

II. Design of Thermal Management System With Two-Phase Flow

A. MHS for SiC MOSFET Power Module

Fig. 1 shows the schematic of a SiC power module assembled on one MHS with flow boiling bubbles. Thermal interface material (TIM) is used between the power module and the MHS to reduce the contact resistance. The heat generated by SiC MOSFETs can be absorbed by taking full advantage of the latent heat of liquid R1234yf while vaporizing in the MHS. An MTMS is required to realize the phase change and heat absorption in the MHS.

B. MTMS Design

Fig. 2(a) and (b) illustrates the experimental measurement platform and schematic diagram of the designed MTMS. The system mainly consists of MHS1 and MHS2 connected in series, a gas flowmeter, a miniature compressor, a condenser, a throttling device, and accessory measurement components. All the components were connected through copper tubes and fittings.

In the system, the compressor was used to increase the pressure of the refrigerant, while the throttling device was to reduce the pressure of the refrigerant and control the flow. The system was divided into a high-pressure (HP) region and a low-pressure (LP) region by the two components. The two MHSs and the gas

TABLE I
SIZES OF MHS

Part	Size (mm)
MHS	50×50×9
Base plate	50×50×1
Cover plate	50×50×1
Chamber	30×30×7
Plate fin	20×0.5×6
Channel spacing	0.5
Inner diameter of tube	5.35
Outer diameter of tube	6.35

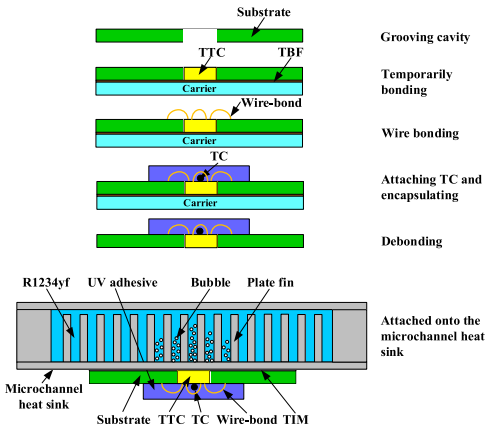

Fig. 3. Packaging of TTV1 and assembly process on MHS.

flowmeter were in the LP region, whereas the condenser lay in the HP region.

The temperatures at the connection tubes of the LP region could be reduced from –10 to –20 °C when the system was operating. To avoid the effect of heat loss on the cooling performance of the system due to the large temperature difference between the connection tubes and the ambient, the connection tubes in the LP region were protected with rubber foam tubes, as shown in Fig. 2(a).

The MHS is a highly compact and lightweight Al plate fin evaporator. It has one inlet and one outlet tubes. The detailed size of MHS is given in Table I. A single MHS, denoted as MHS1, was used in Sections III-A to III-D, whereas two MHSs, denoted as MHS1 and MHS2, were used in Section III-E.

C. TTVs Design

Currently, thermal test chip (TTC) using SiC is not available in the market. To evaluate the cooling performance of the MTMS system, Si-based TTC from Thermal Engineering Associates, Inc., was used to evaluate the cooling performance of MTMS. The size of a single TTC was 2.5 × 2.5 × 0.625 mm^3, which had two resistors in the same layer and four diodes in the other layer. The two resistors covered more than 85% of the chip area. The electrical resistance of each resistor was 7.6 Ω ±10%.

Two TTVs based on substrate embedded packaging technology were designed and fabricated [28]. The detailed process of packaging of TTV1 with one chip and assembly on the MHS is shown in Fig. 3. A TTC was picked and placed in the center cavity of a substrate with the almost same thickness as the TTC,

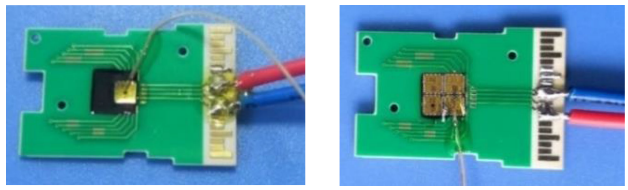

Fig. 4. TTV samples. (a) TTV1. (b) TTV2

and temporarily bonded onto a substrate carrier through a layer of temporary bond film. The two resistors of TTC in the TTV1 were connected in series and then bonded onto one edge of the substrate through gold wires. The total electrical resistance of the TTV1 reached about 15.2 Ω. A thermocouple (TC) was directly attached to the top surface of TTC so that the junction temperature could be precisely monitored in real-time when it was operating. The TTC and TC were then encapsulated by ultraviolet adhesive to protect from damage. After that, the TTV1 was debonded from the carrier.

For TTV2 with multichips, it consisted of four TTCs in a 2 × 2 array without extra spacing. The eight resistors in the four TTCs were connected in series and then bonded to one edge of the substrate through gold wires. Compared with the TTV1, the effective area and the total electrical resistance of the TTV2 increased by four times, which were 0.25 cm^2 and 60.8 Ω, respectively. The TTV1 and TTV2 samples are shown in Fig. 4(a) and (b), respectively.

The TTV was directly attached to the bottom center of MHS through a layer of TIM. The TIM (TC-5888) from Dow Corning was used, which combined advantages of high thermal conductivity (5.2 W/m·K) and thin bond line thickness of approximately 20 μm, which yielded a low specific thermal resistance of 0.05 °C·cm^2/W.

D. Other Components

A miniature rotary compressor (14-24-000X) from Aspen was used in the system, which is the smallest and lightest compressor available in the market as far as we know. Its suction volume was 1.4 cm^3, and the maximum rotational speed was up to 6500 rpm, which can be adjusted by a variable resistor. The pressure and flow rate of refrigerant thus could be adjusted through the variable resistor.

A throttling device played a dual role in regulating the pressure drop across the throttling device and the flow rate and preventing the large pressure drop oscillations across the test module.

For the condenser, an Al minichannel heat exchanger was adopted, which was fabricated based on the miniend milling process. To improve the convective heat transfer coefficient, a fan was applied to the condenser.

To accurately evaluate the cooling performance of the thermal management system, temperature, pressure, and other measurement components were connected to the system. Six high precision Type K TCs (T1-T6) from OMEGA were to monitor the temperatures at different locations of the system. One of the attached locations is shown in Fig. 2(b). The positive and

negative leads of the six TCs were connected to a high-resolution data acquisition device from National Instruments. We could read real-time temperatures via LabVIEW software. Before testing, the signals of TCs were calibrated, and the reference temperature was set to 20 °C.

Two voltage output pressure transducers (PX309-200 G5V) from OMEGA were adopted to detect the pressures of the HP region and LP region, respectively. The absolute pressure range of the transducer was 0–14 bar, and the driver voltage/current was 5 V/0.1 A. The pressure changes in the evaporators were negligible compared to those in the throttling device and miniature compressor [34], so the two pressure transducers could provide the important data needed to assess the system performance. The pressures could be read in realtime in the form of voltages by a digit multimeter from KEYSIGHT. The calibration curve of the pressure P_{PT} (bar) and the tested voltage U_{PT} (V) is expressed as follows [28]:

$$P_{PT} = 2.32 \times U_{PT} + 0.565. \quad (1)$$

We could also indirectly acquire the rotational speed of the compressor via the digit multimeter. The voltage of the variable resistor U_{VR} (V) could be read when the compressor was operating. The rotational speed of compressor n (rpm) then can be calculated as follows:

$$n = \begin{cases} 0 \ (4.3V \le U_{\mathrm{VR}} < 5V) \\ 7078.93 - 1157.89U_{\mathrm{VR}} \ (0.5V \le U_{\mathrm{VR}} \le 4.3V) \\ 6500 \ (U_{\mathrm{VR}} < 0.5V). \end{cases} \quad (2)$$

The gas flowmeter (FMA-4312) from OMEGA was used to monitor the vapor flow rate of refrigerant, which could be read in the electronic display. The driver voltage/current was 5 V/0.09 A. The flow rate range was 0–10 L/min.

The temperatures at different positions, the pressures of HP and LP regions, the flow rate of refrigerant, and the rotational speed of compressor could be recorded in realtime. The system would have a better cooling performance only if these parameters were properly controlled.

E. Thermodynamic Analysis of R1234yf Refrigerant

R1234yf from Honeywell was selected as the refrigerant and filled into the system. Fig. 5 shows the variation of pressure with the saturation temperature of R1234yf. The fit function is expressed as follows:

$$P_s = \exp\left(1.14119 + 0.03326T_s - 9.33109 \times 10^{-5}T_s^2\right) \quad (3)$$

where T_s is the saturation temperature of R1234yf and P_s is the corresponding pressure. As seen in the figure, the pressure of the refrigerant rises nearly quadratically with the saturation temperature. Under the same temperature, reducing the pressure can make the refrigerant change from liquid to vapor, and thus absorb a large amount of heat. Likewise, increasing the pressure can make the refrigerant change from vapor to liquid, and thus release a lot of heat.

Fig. 6 shows a representative experimental working cycle of R1234yf in the system. An ideal pressure–enthalpy diagram of R1234yf was dotted in the figure, which was divided into the subcooled liquid, the liquid/vapor mixture, and the superheated vapor regions by a saturated liquid curve and a saturated vapor curve. The points 1–4 in Fig. 6 correspond to the system locations 1, 2, 3, and 4 shown in Fig. 2.

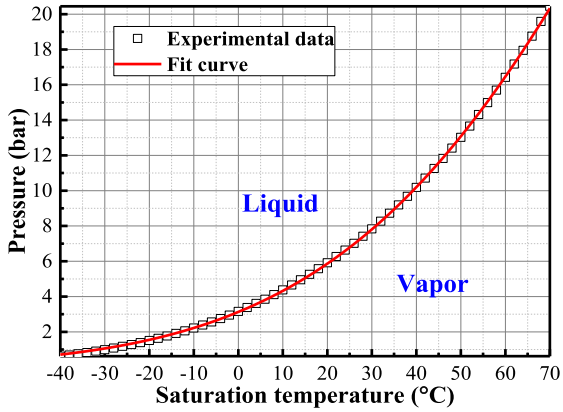

Fig. 5. Variation of pressure with a saturation temperature of R1234yf.

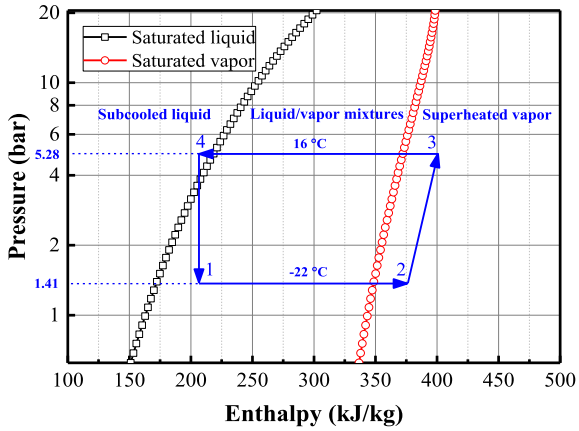

Fig. 6. Representative experimental working cycle of R1234yf in the system.

As shown in Fig. 6, in the process 1–2, most of the heat generated by the TTV is absorbed by the liquid/vapor mixtures of R1234yf due to the vaporization of liquid refrigerant. The bubble grows and departs at a high frequency, forming bubble flow and then slug flow in the microchannels between the plate fins of the MHS. The liquid/vapor mixtures fully change to the superheated vapor after heating. Then, the superheated vapor enters a gas flowmeter. Then, the superheated vapor goes to a compressor and is compressed to a higher pressure vapor, resulting in a higher temperature in the process 2–3. Next, the compressed vapor R1234yf flows into a condenser, the superheated vapor changes to the subcooled liquid. The heat accumulated in the previous processes (1–3) is released to the ambient due to the latent heat of condensation of vapor refrigerant in the process 3–4. Finally, the subcooled liquid refrigerant returns into the MHS1 through a throttling device, the subcooled liquid refrigerant changes into the liquid/vapor mixtures again, and the pressure drops drastically to a low level (process 4–1).

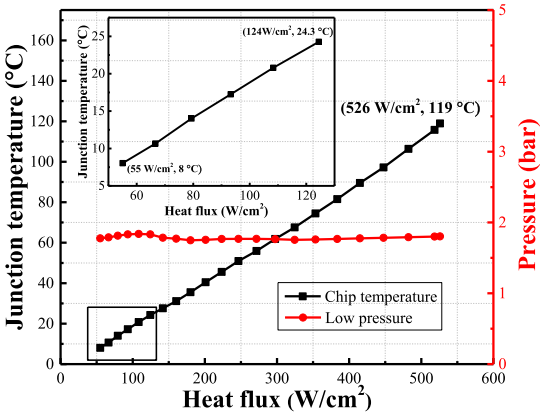

Fig. 7. Junction temperature of TTV1 and pressure of LP region dependent on heat flux of TTV1.

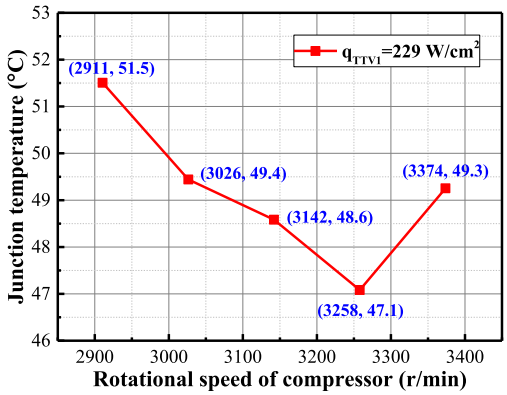

Fig. 8. Junction temperature of TTV1 dependent on the rotational speed of the compressor.

III. Results and Discussion

A. Cooling Performance Evaluation With TTV1

In this section, the cooling performance of the MTMS was evaluated using TTV1. The measured electrical resistance of the TTV1 was 13.76 Ω through a digit multimeter. A 200 V/60 A dc power supply was adopted to drive the TTV1. The heat fluxes rising from 55 to 526 W/cm^2 were tested by increasing the current from 0.5 to 1.51 A.

Fig. 7 displays that the junction temperature of TTV1 and the pressure of the LP region are dependent on the heat flux of TTV1. As seen in the figure, the junction temperature of TTV1 increased almost linearly with the heat flux of TTV1. Particularly, when the heat flux of TTV1 increased from 55 to 124 W/cm^2 (seen from inset), the junction temperature of TTV1 rose from 8 to 24.3 °C, which was below the ambient temperature of 25 °C. As shown in the figure, the pressure of the LP region remained about 1.8 bar. Combining (3) with Fig. 5, the saturation temperature of R1234yf at 1.8 bar was estimated to be –16 °C. This means the junction temperature of TTV1 could be lower than the ambient temperature of 25 °C even when the heat flux of TTV1 reached 124 W/cm^2. On the other hand, when the heat flux of TTV1 increased to 526 W/cm^2, the junction temperature of TTV1 approached to 119 °C, which was near the allowed highest junction temperature 125 °C. For SiC devices with a higher junction temperature, e.g., 175 °C [33], the heat dissipation of the present system could go up to 750 W/cm^2 based on the same level of thermal resistance. Therefore, the thermal management system could dissipate a heat flux of 526 W/cm^2 while maintaining the junction temperature below 120 °C.

B. Effect of the Rotational Speed of the Compressor

In this section, the effect of the rotational speed of the compressor on the cooling performance of the system was analyzed under the same heat flux of TTV1. The rotational speed of the compressor was changed by adjusting the voltage of a variable resistor connected to the compressor controller. According to (2), when the voltage of the variable resistor decreased from 3.6 to 3.2 V, the rotational speed increased from 2911 to 3374 r/min.

Fig. 8 illustrates that the junction temperature of TTV1 is dependent on the rotational speed of the compressor under the heat flux of 229 W/cm^2. From the figure, it can be seen that the junction temperature of TTV1 first decreased and then increased with the rotational speed of the compressor. When the rotational speed of the compressor reached 3258 r/min, the junction temperature of TTV1 went down to 47.1 °C, which was lowered by 4.4 °C compared with the rotational speed of 2911 r/min. During the system operation, the phase-change heat transfer of R1234yf is depended on its flow rate and system pressure drop that could be controlled by adjusting the rotational speed of the compressor. Therefore, the rotational speed of the compressor could affect the cooling performance of the system. Either too high or too slow flow rate would adversely affect cooling performance. In the following investigations, the rotational speed of the compressor was fixed to be 3258 r/min.

C. Effect of the Opening of the Throttling Device

In this section, the effects of changing the opening of the throttling device at the beginning and the testing process on the cooling performance were analyzed, respectively.

For changing the opening at the beginning, by applying the current from 0.5 to 1.4 A, the heat flux of the TTV1 increased from 55 to 449 W/cm^2 in the conditions of a small opening and a large opening, respectively. Fig. 9 shows that the pressure drops across the throttling device and the junction temperatures are dependent on the heat flux of TTV1 under both the small and large openings of the throttling device. As seen in the figure, the pressure drop across the throttling device was affected by the opening of the throttling device. A smaller opening led to a higher pressure drop. The pressure drops were about 4 bar and 3.1 bar under the small and large opening, respectively, and a smaller opening led to a higher pressure drop. In other words, the opening of the throttling device can be quantitatively represented by its pressure drop.

As shown in Fig. 9, when the heat flux of the TTV1 increased from 55 to 353 W/cm^2, the junction temperatures of the TTV1 under the pressure drop of 4 bar were lower than that under the pressure drop of 3.1 bar. When continuing to increase the heat

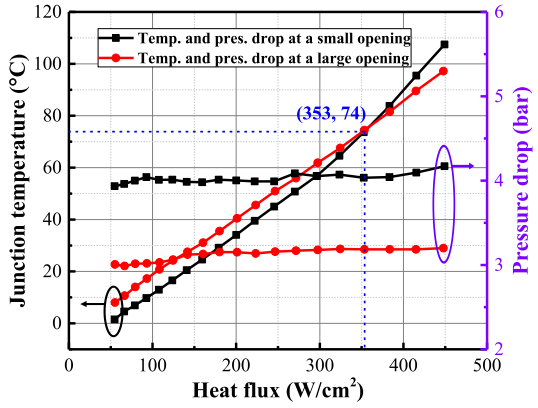

Fig. 9. Pressure drops across the throttling device and junction temperature dependent on the heat flux of TTV1 under different openings of the throttling device.

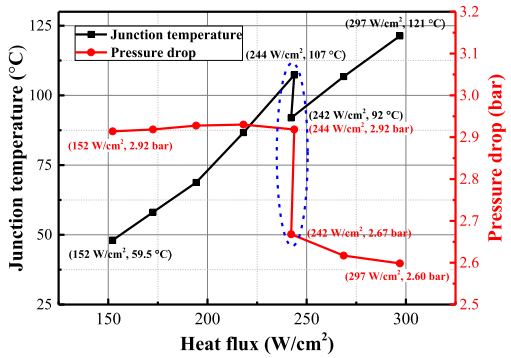

Fig. 10. Effect of the opening of throttling device on junction temperature of TTV2 and pressure drop across the throttling device.

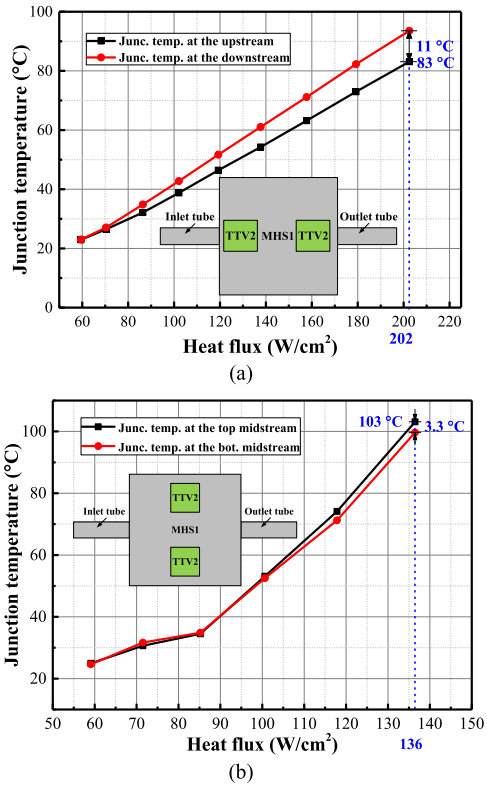

Fig. 11. Junction temperatures of two TTV2s layouts on MHS1. (a) Upstream and downstream. (b) Lateral midstream.

flux of the TTV1, the junction temperature of the TTV1 under the pressure drop of 4 bar surpassed that under the pressure drop of 3.1 bar. Because only a small portion of refrigerants flew into the MHS1 under the pressure drop of 4 bar, complete phase change of the fluid refrigerant could occur, the system showed better cooling performance at lower heat flux but deteriorated at high heat flux. This could be due to the lower flow rate in the MHS1, which could reach the dry-out limit at higher heat flux. As such, increasing the opening of the throttling device could increase the flow rate and reduce the junction temperature of the TTV1 at high heat flux, thus improving the cooling performance of the thermal management system.

For changing the opening at the testing process, by applying the current from 0.8 to 1 A and then from 1 to 1.1 A, the heat flux of TTV2 increased from 152 to 244 W/cm^2 and then from 242 to 297 W/cm^2. Fig. 10 shows the effect of the opening of the throttling device on the junction temperature of TTV2, the pressure drop across the throttling device. When the heat flux of TTV2 increased from 152 to 244 W/cm^2, the junction temperature of TTV2 rose from 59.5 to 107 °C, and the pressure drop almost kept 2.92 bar. The refrigerant was approaching to the dry-our regime due to the lower flow rate. At this moment, the opening of the throttling device was increased to observe its effect on cooling performance. The junction temperature and pressure drop significantly dropped, which decreased from 107 °C, 2.92 bar to 92 °C, 2.67 bar, respectively. Because new R1234yf flew into the MHS1 and more phase-change occurred, the cooling performance of the system was improved. Therefore, when the refrigerant is approaching the dry-out regime, the junction temperature of TTV2 can be reduced by increasing the opening of the throttling device at high heat flux, which allows more refrigerant into MHS and, thus, improves the cooling performance of the system without reaching the dry-out regime.

D. Effect of TTV Layout on MHS1

In this section, the junction temperature distributions of two TTV2 layouts on MHS1 were studied.

In the first layout, two TTV2s were arranged at the upstream and downstream along the centerline of MHS1, and their heat fluxes were both increased from 59 to 202 W/cm^2. Fig. 11(a) shows the junction temperatures of the two TTV2s. As can be seen from the figure, when the heat flux of TTV2 reached 202 W/cm^2, the junction temperature of TTV2 at the upstream was 11 °C lower than at the downstream. The heat generated by TTV2 was conducted through the chip, TIM, and MHS1 base to the chamber, making the liquid refrigerant between plate fins to vaporize. The phase change could provide higher heat convection coefficients. The lower junction temperature of TTV2 at the upstream was due to the better cooling at the upstream with the fresh cold refrigerant, whereas the refrigerant was preheated to vaporize to some degree due to heat spreading

effect, unfavorably affecting the cooling performance at the downstream.

In the second layout, two TTV2s were arranged at the lateral midstream, symmetrically to the centerline of the MHS1, and the heat fluxes were both increased from 59 to 136 W/cm^2. Fig. 11(b) illustrates the junction temperatures of the two TTV2s, which were nearly the same. The junction temperature differential for the two lateral positions was only 3.3 °C, even at the heat flux of 136 W/cm^2. However, compared with the case arranged at the upstream and downstream, the heat dissipation capacity of the system with TTV2s arranged at the lateral midstream was greatly reduced, which was attributed to the reduced flow distribution at the lateral channels instead of centerline channels. Therefore, for two TTVs with the same heat flux, it is suggested to allocate the TTVs at the two lateral positions; for multiple TTVs with different heat flux, it is recommended to put the TTVs at the centerline in the order of decreasing heat fluxes, with the highest one allocated at the upstream.

E. Effect of a Downstream TTV1 on MHS2

In this section, both MHS1 and MHS2 were used. A downstream TTV1 on MHS2 was introduced to study its effect on the pressure drop across the throttling device and junction temperature of the upstream TTV1 on MHS1. The downstream TTV1 could be viewed as either a regular heat-dissipating device or a superheating device. The liquid R1234yf was expected to vaporize more completely in MHS2 upon absorbing heat from the downstream TTV1, thus increasing the enthalpy change of R1234yf before flowing into the condenser.

In the experiment, two 72 V/1.2 A dc power supplies were used to drive the two TTV1s, respectively. By applying the current from 0.5 to 1.15 A, the heat fluxes of both TTV1s were increased from 55 to 297 W/cm^2.

Fig. 12(a) shows that the pressure drops across the throttling device is dependent on the heat flux of upstream TTV1 when a downstream TTV1 is used as a heat-dissipating device and a superheating device, respectively. As seen from the figure, the pressure drop across the throttling device in the system with a downstream superheating TTV1 was higher than that with a downstream heat-dissipating TTV1. The pressure differential increased slightly with the heat flux of the upstream TTV1. As discussed in Section III-C, a smaller opening of the throttling device led to a higher pressure drop. Therefore, the downstream TTV1 could be a heat-dissipating device or superheating device, which was determined by the pressure drop across the throttling device.

Fig. 12(b) shows the effect of a downstream TTV1 on the junction temperatures of TTV1s. Compared with the upstream TTV1 followed by a regular heat-dissipating TTV1, the junction temperature of the upstream TTV1 followed by a superheating TTV1 dropped by 8 °C when their heat fluxes increased to 297 W/cm^2. Nonetheless, the junction temperature of the superheating TTV1 increased evidently, which increased to 92 °C. Because a few refrigerants flew into the MHSs under the HP-drop across the throttling device, the liquid R1234yf was vaporized more completely in MHS2 upon absorbing heat from

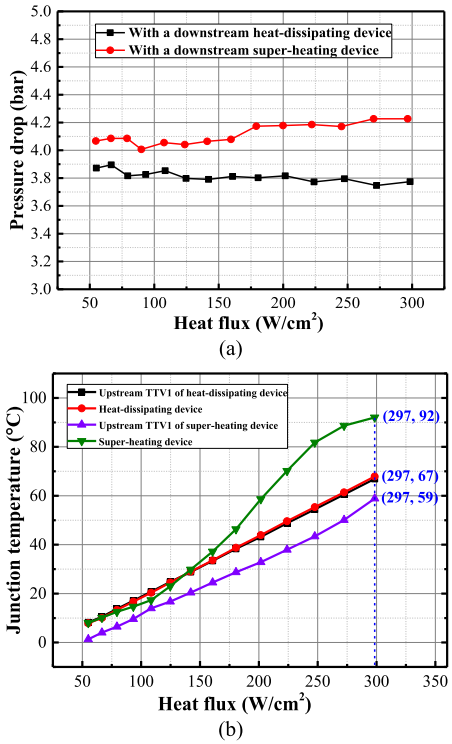

Fig. 12. Effect of a downstream TTV1 on MHS2. (a) Pressure drops across the throttling device. (b) Junction temperatures of TTV1s.

the downstream TTV1, thus increasing the enthalpy change of R1234yf. Therefore, the upstream TTV1 followed by a superheating TTV1 showed a lower junction temperature than that followed by a heat-dissipating TTV1. The refrigerant in the MHS2 was preheated to vaporize to some degree, unfavorably leading to the higher junction temperature of superheating TTV1 than that of the heat-dissipating TTV1. The junction temperature of the heat-dissipating TTV1 was close to that of the upstream TTV1, but their temperatures were higher than that of the upstream TTV1 followed by a superheating TTV1. Because enough refrigerant flew into the MHSs under the LP-drop across the throttling device, the phase-change rate was almost the same in the two MHSs. Therefore, the downstream TTV1 on MHS2 could function as a superheating device while making the junction temperature of the upstream TTV1 on MHS1 at a lower value.

F. Discussion on Cooling Performance Enhancement

In this article, various effect factors were studied to improve the cooling performance of the thermal management system. However, there is still some room to improve.

1) A superheating device can also be called as a sacrificed device, which can help to improve the cooling performance of the system.
2) In this experiment, we found that the filling amount of R1234yf affected the cooling performance of the MTMS. Either over-filled or under-filled refrigerants would cause

deterioration in cooling performance. A more detailed study on the filling amount will be conducted.

3) Compared with the air-cooled condenser, a liquid-cooled condenser could improve the heat transfer capability from the system to the ambient. To achieve much better cooling performance, the liquid-cooled condenser will be used in the future.
4) In this experiment, a throttling device with a wide range of openings was used. However, only in the last turn, did the adjustment of the opening could affect the cooling performance. In the future study, a thermal expansion valve will be used to achieve precise control of the pressure drop. The maximum operating pressure of the thermal expansion valve should be slightly larger than the highest pressure of the present system. To study the effect of the opening of the throttling device on the cooling performance, an electrically controlled valve with program control will replace the throttling device in the present system.
5) Further study on the affecting factors will be performed. Microchannel structures and inlet and outlet of the MHS will be optimized via computational fluid dynamics simulation. The effect of the mass flow rate of refrigerant on the cooling performance of the system will be studied.
6) Single-sided MHS with two-phase flow boiling has been proved to be an effective cooling solution for high heat-flux TTV. If double-sided cooling is adopted, much more heat can be absorbed.

With the above-mentioned improvement techniques, the cooling performance of the system can further be improved to address the more demanding heat dissipation level and cover even higher heat flux level of 1000 W/cm^2 for the SiC MOSFET power modules.

IV. Conclusion

In this article, we developed an MTMS with the two-phase flow. Single/multiple Si TTCs were packaged in the center cavity of a substrate. Thus, the TTCs in the TTVs could be directly attached to an MHS through a layer of TIM. To realize the two-phase flow in the system, low boiling-point R1234yf with environmental friendliness was selected to fill into the system. The system mainly consisted of two identical Al MHSs, a miniature compressor, a condenser, a throttling device, and temperature, pressure, and accessory measurement components. The cooling performance of the system with one single-chip TTV1 was analyzed first. The experimental results showed that the MTMS could dissipate up to 526 W/cm^2 while maintaining the junction temperature of TTV1 below 120 °C. For SiC devices with a junction temperature, e.g., 175 °C, the current system is predicted to dissipate the heat flux as high as about 750 W/cm^2. Then, the effects of the rotational speed of the compressor, the opening of the throttling device, TTV layout on MHS1, and a downstream heater on MHS2 on the cooling performance of the system were analyzed sequentially. The study showed that the opening of the throttling device had a great effect on cooling performance. For the multimodule system, the chip at the upstream had the best cooling performance. On the other hand, the downstream TTV on MHS2 could function as a superheating device instead of a heat-dissipating device, making the junction temperature of upstream TTV at a low value.

References

[1] P. Wang, P. McCluskey, and A. Bar-Cohen, "Two-phase liquid cooling for thermal management of IGBT power electronic module," *J. Electron. Packag.*, vol. 135, pp. 021001-1–021001-11, Jun. 2013.

[2] P. Wang, P. McCluskey, and A. Bar-Cohen, "Hybrid solid- and liquid-cooling solution for isothermalization of insulated gate bipolar transistor power electronic devices," *IEEE Trans. Compon., Packag. Technol.*, vol. 3, no. 4, pp. 601–611, Apr. 2013.

[3] I. Aranzabal, I. M. de Alegría, N. Delmonte, P. Cova, and I. Kortabarria, "Comparison of the heat transfer capabilities of conventional single- and two-phase cooling systems for an electric vehicle IGBT power module," *IEEE Trans. Power Electron.*, vol. 34, no. 5, pp. 4185–4194, May 2019.

[4] S. N. Joshi and E. M. Dede, "Two-phase jet impingement cooling for high heat flux wide band-gap devices using multi-scale porous surfaces," *Appl. Therm. Eng.*, vol. 110, pp. 10–17, Jan. 2017.

[5] A. Bar-Cohen, J. D. Albrecht, and J. J. Maurer, "Near-junction thermal management for wide bandgap devices," in *Proc. IEEE Compound Semicond. Integr. Circuit Symp.*, Waikoloa, HI, USA, Nov. 2011, pp. 1–5.

[6] E. Laloya, Ó. Lucía, H. Sarnago, and J. M. Burdío, "Heat management in power converters: From state of the art to future ultrahigh efficiency systems," *IEEE Trans. Power Electron.*, vol. 31, no. 11, pp. 7896–7908, Nov. 2016.

[7] S. Wiriyasart and P. Naphon, "Fill ratio effects on vapor chamber thermal resistance with different configuration structures," *Int. J. Heat Mass Transf.,* vol. 127, pp. 164–171, Dec. 2018.

[8] J. Zeng *et al.*, "Experimental investigation on thermal performance of Al vapor chamber using micro-grooved wick with reentrant cavity array," *Appl. Therm. Eng.*, vol. 130, pp. 185–194, Feb. 2018.

[9] I. Mudawar, D. Bharathan, K. Kelly, and S. Narumanchi, "Two-phase spray cooling of hybrid vehicle electronics," *IEEE Trans. Compon., Packag. Technol.*, vol. 32, no. 2, pp. 501–512, Jun. 2009.

[10] D. W. Yang, Y. Wang, G. F. Ding, Z. Y. Jin, J. H. Zhao, and G. L. Wang, "Numerical and experimental analysis of cooling performance of single-phase array MHSs with different pin-fin configurations," *Appl. Therm. Eng.*, vol. 112, pp. 1547–1556, Feb. 2017.

[11] H. Y. Zhang, D. Pinjala, T. N. Wong, K. C. Toh, and Y. K. Joshi, "Single-phase liquid cooled MHS for electronic packages," *Appl. Therm. Eng.*, vol. 25, pp. 1472–1487, Jul. 2005.

[12] H. Y. Zhang, D. Pinjala, Y. K. Joshi, T. N. Wong, and K. C. Toh, "Development and characterization of thermal enhancement structures for single-phase liquid cooling in microelectronics systems," *Heat Transfer Eng.*, vol. 28, pp. 997–1007, Dec. 2007.

[13] N. Blet, S. Lips, and V. Sartre, "Heats pipes for temperature homogenization: A literature review," *Appl. Therm. Eng.*, vol. 118, pp. 490–510, May 2017.

[14] Z. H. Wu and R. Du, "Design and experimental study of a miniature vapor compression refrigeration system for electronics cooling," *Appl. Therm. Eng.*, vol. 31, pp. 385–390, 2011.

[15] X. C. Tong, *Advanced Materials for Thermal Management of Electronic Packaging*. New York, NY, USA: Springer, 2011.

[16] G. Tang, Y. Han, B. L. Lau, X. Zhang, and D. M. W. Rhee, "Development of a compact and efficient liquid cooling system with silicon microcooler for high-power microelectronic devices," *IEEE Trans. Compon., Packag. Technol.*, vol. 6, no. 5, pp. 729–739, May 2016.

[17] Y. Han, B. L. Lau, H. Zhang, and X. Zhang, "Package-level Si-based micro-jet impingement cooling solution with multiple drainage micro-trenches," in *Proc. IEEE 16th Electron. Packag. Technol. Conf.*, Singapore, 2014, pp. 330–334.

[18] M. Tawk, Y. Avenas, A. Kedous-Lebouc, and M. Petit, "Numerical and experimental investigations of the thermal management of power electronics with liquid metal mini-channel coolers," *IEEE Trans Ind. Appl.*, vol. 49, no. 3, pp. 1421–1429, May/Jun. 2013.

[19] M. Tawk, Y. Avenas, A. Kedous-Lebouc, and M. Petit, "Study and realization of a high power density electronics device cooling loop using a liquid metal coolant," in *Proc. IEEE Energy Convers. Congr. Expo.*, Phoenix, AZ, USA, 2011, pp. 36–43.

[20] M. Hodes, R. Zhang, L. S. Lam, R. Wilcoxon, and N. Lower, "On the potential of galinstan-based minichannel and minigap cooling," *IEEE Trans. Compon., Packag. Technol.*, vol. 4, no. 1, pp. 46–56, Jan. 2014.

[21] A. Heinzel *et al.*, "Liquid metals as efficient high-temperature heat-transport fluids," *Energy Technol.*, vol. 5, pp. 1026–1036, Feb. 2017,

[22] E. M. Fayyadh, M. M. Mahmoud, K. Sefiane, and T. G. Karayiannis, "Flow boiling heat transfer of R134a in multi microchannels," *Int. J. Heat Mass Transf.*, vol. 110, pp. 422–436, Jul. 2017.

[23] T. G. Karayiannis and M. M. Mahmoud, "Flow boiling in microchannels: Fundamentals and applications," *Appl. Therm. Eng.*, vol. 115, pp. 1372–1397, Mar. 2017.

[24] I. Mudawar, "Two-phase MHSs: Theory, applications, and limitations," *ASME J. Electron. Packag.*, vol. 133, pp. 041002-1–041002-31, Dec. 2011.

[25] C. Falsetti, M. Magnini, and J. R. Thome, "Hydrodynamic and thermal analysis of a micro-pin fin evaporator for on-chip two-phase cooling of high density power micro-electronics," *Appl. Therm. Eng.*, vol. 130, pp. 1425–1439, Feb. 2018.

[26] K. Liang, Z. H. Li, M. Chen, and H. Y. Jiang, "Comparisons between heat pipe, thermoelectric system, and vapour compression refrigeration system for electronics cooling," *Appl. Therm. Eng.*, vol. 146, pp. 260–267, Jan. 2019.

[27] J. He *et al.*, "Experimental study of a miniature vapor compression refrigeration system with two heat sink evaporators connected in series or in parallel," *Int. J. Refrigeration*, vol. 49, pp. 28–35, Jan. 2015.

[28] F. Hou *et al.*, "Evaluation of a compact two-phase cooling system for high heat flux electronic packages," *Appl. Therm. Eng.*, vol. 163, Dec. 2019, Art. no. 114338.

[29] J. Navarro-Esbrí, J. M. Mendoza-Miranda, A. Mota-Babiloni, A. Barragán-Cervera, and J. M. Belman-Flores, "Experimental analysis of R1234yf as a drop-in replacement for R134a in a vapor compression system," *Int. J. Refrigeration*, vol. 36, pp. 870–880, May 2013.

[30] Z.H. Li, K. Liang, and H.Y. Jiang, "Experimental study of R1234yf as a drop-in replacement for R134a in an oil-free refrigeration system," *Appl. Therm. Eng.*, vol. 153, pp. 646–654, May 2019.

[31] J. Sieres and J. M. Santos, "Experimental analysis of R1234yf as a drop-in replacement for R134a in a small power refrigerating system," *Int. J. Refrigeration*, vol. 91, pp. 230–238, Jul. 2018

[32] A. Mota-Babiloni, J. Navarro-Esbrí, Á. Barragán, F. Molés, and B. Peris, "Drop-in energy performance evaluation of R1234yf and R1234ze(E) in a vapor compression system as R134a replacements," *Appl. Therm. Eng.*, vol. 71, pp. 259–265, Oct. 2014.

[33] CREE, CPM2-1200-0025B, Rev. C. [Online]. Available: https://www.wolfspeed.com/power/products/sic-mosfets/cpm2-1200-0025b, Accessed on: Jan. 2016.

[34] R. Mongia *et al.*, "Small scale refrigeration system for electronics cooling within a notebook computer," in *Proc. Therm. Thermomech. Proc. 10th Intersociety Conf. Phenomena Electron. Syst.*, 2006, pp. 751–758.